applied sciences

MDPI

Article

Comparative Study of In Situ TiO_2 Generation for the Degradation of "Deiman Navy Blue" Dye

Diana I. Cuautle-Lezama [1], Felipe M. Galleguillos-Madrid [2,*], Susana Leiva-Guajardo [2], Anselmo Osorio-Mirón [1], V. E. Reyes-Cruz [3], Martin Reyes-Pérez [3], Marinka Varas [2], Norman Toro [4] and Jose A. Cobos-Murcia [3,*]

[1] Torre de Ingeniería, Facultad de Ciencias Químicas-Orizaba, Universidad Veracruzana, Orizaba 94340, Mexico; m22201114@pachuca.tecnm.mx (D.I.C.-L.); anosorio@uv.mx (A.O.-M.)
[2] Centro de Desarrollo Energético de Antofagasta, Universidad de Antofagasta, Av. Universidad de Antofagasta 02800, Antofagasta 1271155, Chile; susana.leiva.guajardo@ua.cl (S.L.-G.); mvaras@uantof.cl (M.V.)
[3] Instituto de Ciencias Básicas e Ingeniería, Universidad Autónoma del Estado de Hidalgo, Carr. Pachuca—Tulancingo km. 4.5, Mineral de la Reforma 42184, Mexico; profe_4948@uaeh.edu.mx (V.E.R.-C.); mreyes@uaeh.edu.mx (M.R.-P.)
[4] Faculty of Engineering and Architecture, Universidad Arturo Prat, Iquique 1110939, Chile; notoro@unap.cl
* Correspondence: felipe.galleguillos.madrid@uantof.cl (F.M.G.-M.); jose_cobos@uaeh.edu.mx (J.A.C.-M.)

Abstract: This study presents the development and application of a batch-type photoelectrochemical reactor employing advanced oxidation processes (AOPs) with in situ generated TiO_2 particles for the efficient degradation of azo dyes. The reactor uses titanium sheets as electrodes, facilitating the electrochemical generation of TiO_2, which acts as a photocatalyst under UV light. This study specifically targets azo dyes frequently encountered in industrial wastewater, focusing on Brilliant Blue, Erythrosine, and Tartrazine, which together form the Navy Blue dye composition. The experimental methodology replicates real-world conditions, ensuring the results are representative of practical scenarios. Key findings demonstrate that the in situ production of TiO_2 enables effective heterogeneous photocatalysis, achieving significant dye degradation rates. This research highlights the novelty of combining in situ TiO_2 generation with a batch-type reactor, offering advantages in cost-effectiveness, scalability, and environmental impact. Comparative analysis with existing methods underscores the reactor's potential for industrial applications, particularly in wastewater treatment. Furthermore, this study outlines the mechanistic insights into dye degradation and provides a foundation for optimizing photocatalytic processes to address environmental challenges.

Keywords: colored waters; heterogeneous photocatalysis; ultraviolet light; TiO_2 in situ

check for updates

Academic Editor: Dino Musmarra

Received: 22 October 2024
Revised: 8 January 2025
Accepted: 9 January 2025
Published: 11 February 2025

Citation: Cuautle-Lezama, D.I.; Galleguillos-Madrid, F.M.; Leiva-Guajardo, S.; Osorio-Mirón, A.; Reyes-Cruz, V.E.; Reyes-Pérez, M.; Varas, M.; Toro, N.; Cobos-Murcia, J.A. Comparative Study of In Situ TiO_2 Generation for the Degradation of "Deiman Navy Blue" Dye. *Appl. Sci.* **2025**, *15*, 1825. https://doi.org/10.3390/app15041825

Copyright: © 2025 by the authors. Licensee MDPI, Basel, Switzerland. This article is an open access article distributed under the terms and conditions of the Creative Commons Attribution (CC BY) license (https://creativecommons.org/licenses/by/4.0/).

1. Introduction

Environmental care, particularly in water preservation, has driven the development of advanced wastewater treatment methods, especially for effluents from industries such as textiles. Colorants, a subset of approximately seventy thousand widely used and five million known contaminating substances globally, pose a significant challenge due to their high molecular weight, complex structures, and high solubility [1,2]. When discharged into water bodies, these substances severely impact aquatic and terrestrial ecosystems, including human health [3]. The rising complexity of dye degradation is attributed to the increasing number of colorant components and their concentrations in wastewater [4]. To address this issue, environmentally friendly methods have been developed, including the application of

photocatalytic reactors and advanced oxidation technologies (AOTs) [5,6]. AOTs have proven effective in reducing the environmental impact of colorants by leveraging solar energy to lower operational costs [7,8]. Among these, heterogeneous photocatalysis using titanium dioxide (TiO_2) has demonstrated exceptional efficiency in degrading dye-contaminated effluents [9–13]. Successful implementation of these methods requires consideration of the water's physicochemical properties [14].

To enhance the understanding of advanced oxidation technologies (AOTs), it is important to differentiate between homogeneous and heterogeneous types. Homogeneous AOTs, such as UV/H_2O_2, Fenton, photo-Fenton, electro-Fenton, UV/$S_2O_8^{2-}$, and UV/HSO_5^-, rely on soluble catalysts or reagents to generate reactive species like hydroxyl radicals for pollutant degradation. These processes are widely used in wastewater treatment and have been shown to be effective in removing pollutants [15–17]. However, one limitation of homogeneous AOTs is the potential for secondary pollution caused by using soluble catalysts, and the need for precise control over reagent concentrations.

On the other hand, heterogeneous AOTs, such as TiO_2 photocatalysis [8], heterogeneous Fenton reagent photocatalysis [9], and plasma degradation processes [18], utilize solid catalysts, which present several advantages. These processes are eco-friendly, as the catalysts are recyclable and have a longer lifespan compared to soluble reagents. Additionally, since no soluble catalysts are used, the risk of secondary pollution is minimized. The main challenge with heterogeneous AOTs, however, lies in the difficulty of separating the solid catalyst from the treated solution after the reaction, which can complicate the recovery and reuse of the catalyst.

By explaining these key differences, this introduction sets the stage for understanding the electrochemical approach used in this study, which offers operational simplicity and adaptability, making it a promising complementary technology to traditional AOTs in wastewater treatment.

TiO_2 is the most widely used photocatalyst due to its high photoactivity, chemical and biological inertness, stability under UV light, low cost, and negligible toxicity [19,20]. Its anatase phase, known for high stability and efficient oxidation reactions, is extensively utilized in environmental applications [21,22]. Efforts to improve TiO_2's performance have focused on extending its efficacy under longer wavelengths, optimizing its reactivity at various pH levels, and enhancing its photocatalytic activity through structural modifications [23,24].

This study proposes a novel approach to the degradation of colorants in industrial wastewater, utilizing a batch-type photoelectrochemical reactor for the in situ generation of TiO_2. Unlike traditional methods, which rely on either photocatalytic or electrochemical processes alone, our reactor integrates both electrochemical processes and homogeneous photocatalysis. This combined approach aims to degrade a range of dyes, including Brilliant Blue, Erythrosine, and Tartrazine, which together form the Navy Blue dye. The novelty of our method lies in its ability to simultaneously generate TiO_2 in situ while maintaining high degradation efficiency and cost-effectiveness. Unlike other TiO_2 production methods that are often costly and energy-intensive, our approach seeks to improve scalability and reduce operational costs, making it more suitable for industrial applications. The central research problem addresses the need for sustainable, efficient, and scalable dye degradation methods in wastewater treatment. The hypothesis guiding this study is that the in situ generation of TiO_2 within a batch-type photoelectrochemical reactor can offer a more sustainable, cost-effective, and efficient solution compared to existing degradation technologies.

2. Materials and Methods

2.1. Photoelectrochemical System

The photoelectrochemical system consisted of a batch-type reactor, where homogeneous photocatalysis in the advanced oxidation process (AOP) was applied for dye degradation. To assemble it, a 500 mL glass beaker was used, its exterior coated with aluminum foil to enhance ultraviolet light absorption. Within the beaker, a 250 mL glass Erlenmeyer flask housed three generic UV LED bulbs with a total power of 9 W, providing a UV light intensity of 810 $\mu W \times cm^{-2}$ and a maximum peak wavelength of 365 nm. Two titanium (Ti) electrodes, in sheet form with a geometric area of 48 cm^2 and an electroactive area of 28.6 cm^2, served as the anode and cathode. These electrodes were electrically polarized using a galvanostatic technique with a BK Precision model 1670A (BK, Mandeville, LA, USA) power source. Subsequent experiments involved UV light exposure, activating the photocatalytic reaction and leading to the in situ production of titanium dioxide (TiO_2). Control experiments without UV light exposure were conducted to assess the photocatalyst's effects in the absence of photoactivation. Rigorous safety measures were adhered to, and comprehensive data, including UV light intensity, current density, and reaction kinetics, were collected to evaluate the system's efficiency in dye degradation. The design showcased the system's potential as an environmentally friendly and cost-effective solution for treating wastewater with dye contaminants.

2.2. Electrode Preparation

The Ti electrodes underwent a preliminary surface mechanical treatment by being uniformly polished with #200 water sandpaper (grits per square inch) from the Fandeli brand. Subsequently, they underwent an ultrasonic cleaning process in deionized water using Cole Parmer 8890 equipment for a duration of 10 min.

2.3. Operating Conditions of the Photoelectrochemical Reactor

The photoelectrochemical reactor was operated under controlled conditions to study the degradation of dye contaminants through photocatalysis. The reactor's performance was influenced by several key parameters, including the applied current density, UV light exposure, and the reaction time. The conditions were optimized to ensure effective photocatalytic degradation while minimizing external variables. The reactor was operated at three different current densities, 0.2, 1.0, and 2.0 $mA \times cm^{-2}$, with the absence of current also considered as a baseline condition. These current densities were selected based on prior studies indicating their relevance in promoting efficient electron transfer during the photocatalytic process. The reactor was exposed to UV light from the LED bulbs (total power of 9 W) to enhance the photocatalytic activity. Control experiments were performed without UV exposure to evaluate the effects of current alone.

The reaction was conducted at ambient temperature and atmospheric pressure, with all experiments carried out in duplicate to ensure reproducibility. During each experiment, samples were taken at regular intervals (every 30 min) to monitor the dye concentration and evaluate the degradation progress. The duration of the experiments was varied depending on the reaction kinetics observed, with typical experiments lasting up to 180 min. The reactor's configuration was designed to ensure uniform exposure of the electrodes to the UV light, and the geometry of the electrodes (Ti sheets with an electroactive area of 28.6 cm^2;) was chosen to optimize the photocatalytic reaction. The electroactive area was sufficient to facilitate efficient electron transfer while maintaining a manageable current density.

The experimental setup was monitored for stability, and parameters such as pH, cell potential, and dye concentration were recorded regularly to ensure consistent operation. This controlled set of operating conditions allowed for a thorough assessment of the sys-

tem's performance in dye degradation and its potential application in wastewater treatment. The effects of both imposed current density and UV light exposure were systematically analyzed to determine the optimal conditions for maximum degradation efficiency.

The temperature was maintained constant throughout the experiments as specified in the methodology, ensuring consistent conditions for evaluating the degradation process. This approach allowed for isolating the effects of the studied variables without interference from temperature fluctuations.

2.4. Dye Preparation and Calibration Curve

The photoelectrochemical reactor and analytical method were developed to address a real-world issue: the degradation of a commercial dye widely used in industry. The chemical composition of such dyes is often protected by industrial property regulations, which adds complexity to their analysis. Consequently, this study aimed to evaluate the composition and proportion of components within a commonly used commercial dye to better understand the system under investigation as a case study for the proposed technology.

To evaluate the reduction in dye concentration during treatment, a 50% solution of a commercial dye was prepared following the manufacturer's recommendations (1 mL per L or kg of the finished product). Specifically, 0.5 mL of the dye was dissolved in deionized water, and 1% sodium chloride (NaCl) was added as a supporting electrolyte to simulate typical dye conditions and enhance the solution's conductivity.

A calibration curve was constructed using six different concentrations, prepared through serial dilutions of the initial solution (0.5 mL $\times$ L^{-1}) using the formula $C_1V_1 = C_2V_2$. The resulting concentrations were 100%, 75%, 50%, 25%, 5%, and 0%, with 0% serving as the blank, using deionized water. Absorbance measurements were performed using a Thermo Scientific NanoDrop One UV-Vis spectrophotometer (Thermo Scientific, Waltham, MA, USA). Wavelength scans were conducted over the range of 190–700 nm to capture the full absorbance spectrum.

To identify and quantify the dyes present in the commercial mixture, the UV-Vis spectra were analyzed at characteristic wavelengths commonly associated with industrial dyes, such as Tartrazine (λ_{max} = 428 nm), Erythrosine (530 nm), and Brilliant Blue (630 nm). While the composition of the commercial dye mixture depends on the manufacturer and may vary, these wavelengths were chosen based on typical dyes widely used in industrial applications. Overlapping peaks in the spectra were deconvoluted using the deconvolution tool in Origin 2024 software. This process allowed precise quantification of individual dye components within the mixture by separating their overlapping spectral contributions.

The calibration curve was generated by plotting the absorbance values at these characteristic wavelengths against the corresponding dye concentrations. Linear regression analysis, performed using Origin 2024, provided the calibration equation and associated statistical parameters (e.g., coefficient of determination, R^2). This information was crucial for ensuring the accuracy and reliability of the calibration.

Changes in dye concentration during the treatment process were monitored by comparing absorbance values at each time interval against the calibration curve. The degradation rates were calculated for each dye based on their specific absorbance maxima. Experimental conditions and parameters during the photoelectrochemical treatment were consistently controlled to ensure reproducibility and validity of the results.

The results are presented as the degradation of the fraction of each dye, highlighting their individual contribution to the overall composition of the commercial mixture. The properties and characteristics of the dyes identified in the commercial product are included, as they form the basis for the discussion of the results. The chemical composition of the dyes was inferred from the experimental evaluation and the manufacturer's specifications

to provide a comprehensive understanding of the system under study. This detailed characterization enhances the relevance of this research as a case study for the application of photoelectrochemical technology to real-world problems.

2.5. Analysis of the Imposed Current and Ultraviolet Light Effects

To assess the responses to the imposed current and UV light effects, a factorial experimental design was employed (Table 1), involving two input variables: (A) the imposition of 0.2, 1, and 2 mA $\times$ cm^{-2} of electric current and no current (control), and (B) with and without exposure to UV light. It is important to note that the control experiments without UV light exposure were conducted under identical conditions to the experimental runs with UV light, except for the UV light source. This ensured that all parameters, such as the dye concentration, solution volume, and experimental setup, remained consistent across both sets of experiments. The output variables assessed included dye degradation, cell potential, obtained mass, and pH. To minimize experimental errors, all experiments were conducted randomly and in duplicate. Multivariate analyses were performed using the NCSS 2007 computational program. The factorial design and selected variables aimed to comprehensively understand the impact of the imposed current and UV light on the photocatalytic system's performance, ensuring the reliability of the results through careful control of variables.

Table 1. Experimental design of operating variables for the photoelectrochemical reactor: (a) current and (b) UV light.

Experiment	I (mA$\times$$cm^{-2}$) (a)	UV Light (b)
1	0.00	YES
2	0.00	NO
3	0.20	YES
4	0.20	NO
5	1.00	YES
6	1.00	NO
7	2.00	YES
8	2.00	NO

2.6. Experimental Conditions and Statistical Analysis

The experiments were conducted using a prototype reactor currently under optimization to evaluate the degradation of commercial dyes under different experimental conditions. The primary variables considered were current imposed (A), UV light (B), and their combined effect (AB). The response variables included the degradation fractions of Tartrazine, Erythrosine, and Brilliant Blue, as well as potential, mass, and pH.

Six replicate measurements were performed for each experimental condition to ensure statistical reliability. Statistical analysis was carried out using multivariate analysis of variance (MANOVA) to assess the significance of the tested factors and their interactions. Roy's Largest Root test was employed to evaluate the statistical significance, with the degrees of freedom (GL1 for factors, GL2 for error), the test value, and the fraction F reported. A probability level of α = 0.15 was selected due to the exploratory nature of this study and the use of a prototype reactor still in the optimization phase. This approach allows for identifying trends and potential interactions that may guide further reactor refinement.

The parameters included in the analysis were chosen based on their relevance to the experimental objectives and their consistent measurement across replicates. These parameters were current, percentage of degradation, mass, and pH. The variability in these measurements, especially in terms of their recorded fluctuations, was carefully considered

to ensure the reliability of the results. In addition, the operational parameters of the reactor were also evaluated for variability, including cell potential, electrical consumption per unit of degraded mass, effective area, space–time efficiency, and current density.

For the reactor operations, under conditions with and without UV light, key efficiency parameters were recorded with corresponding variability. This includes values for cell potential (E_{cell}), electrical consumption per unit of degraded mass (Consumption), effective area (τ_{et}), and current density (j), with observed fluctuations reported. This variability, particularly in the operational parameters such as the effective area and current density, was carefully accounted for in the analysis to provide a complete understanding of reactor performance under different conditions.

The accuracy of the measurements was ensured through instrument calibration, with calibration curves demonstrating high linearity ($R^2 > 0.99$). Repeatability was assessed by maintaining relative standard deviations (RSD) below 5% across replicates, and variability in operational parameters was factored into the experimental conditions to allow for a more comprehensive evaluation of reactor performance.

2.7. Reaction Kinetics

To characterize the reactor's performance during dye degradation with and without UV light exposure, the dye concentration was monitored using UV-Vis spectrophotometry within a wavelength range of 300 to 700 nm. Samples were collected from the reactor every 30 min.

The fraction of degraded dye (f_{deg}) was calculated using Equation (1), where n represents the dye moles of Tartrazine, Erythrosine, and Brilliant Blue, and it is the fraction (f_n) of the remaining dye (Equation (2)) yet to be degraded. Each fraction (Tartrazine, Erythrosine, and Brilliant Blue) was determined by monitoring the decrease in absorbance at the peaks of 428 nm, 530 nm, and 630 nm, respectively.

The fraction of degradation for each dye without UV light was fitted using a zero-order equation (Equation (3)), while with UV light, Equation (4), proposed in this work based on the proposed reaction mechanism, was employed. Here, n is the number of moles, j is the consumed current density, A is the electrode area, F is Faraday's constant, z is the number of transferred electrons, n is the dye mass, k_{elec} is the degradation constant expressed in mol units, and k_{Ox1} and k_{Ox2} are oxidation constants according to the proposed reaction mechanism.

Experimental data were nonlinearly fitted by iteration using the Levenberg–Marquardt algorithm implemented in the Origin 8 computational program. This enabled a thorough understanding of the degradation kinetics and provided valuable insights into the efficiency of the proposed photocatalytic system. The corresponding set of kinetic expressions is presented in Equations (1)–(4):

$$f_{deg} = \sum_{n=n_0} \frac{1}{3}(1 - f_n) \tag{1}$$

$$f_n = \frac{[n]_t}{[n]_0} \tag{2}$$

$$f_{deg} = \frac{jA}{zF[n]_0} K_{el} t \tag{3}$$

$$f_{deg} = \frac{1}{[n]_0}\left(\frac{K_{el}'}{K_{fel}} - e^{\,K_{fel}\,\frac{jA}{zF}\,t}\right) \tag{4}$$

3. Results

Figure 1 shows the UV-Vis spectra obtained from the commercial dye under initial conditions (solid black line) and after treatment with an imposed current density of 2 mA cm^{-2} and UV light (solid purple line). The spectra correspond to Experiment 7 of the experimental design. The dye's absorption bands, which are characteristic of the individual components, were observed at 428, 530, and 630 nm. These wavelengths correspond to the specific dyes present in the commercial mixture: Tartrazine [25], Erythrosine [26], and Brilliant Blue [27], respectively. To analyze the reduction in dye molecules, the spectra were deconvoluted (dashed lines), allowing for the determination of peak values for each absorption band. This analysis provides insight into the extent of dye degradation under the experimental conditions applied. The bathochromic shifts observed are likely to be due to changes in the environment of the chromophore groups, which could be influenced by factors such as pH, solvent, or interactions with other components in the system.

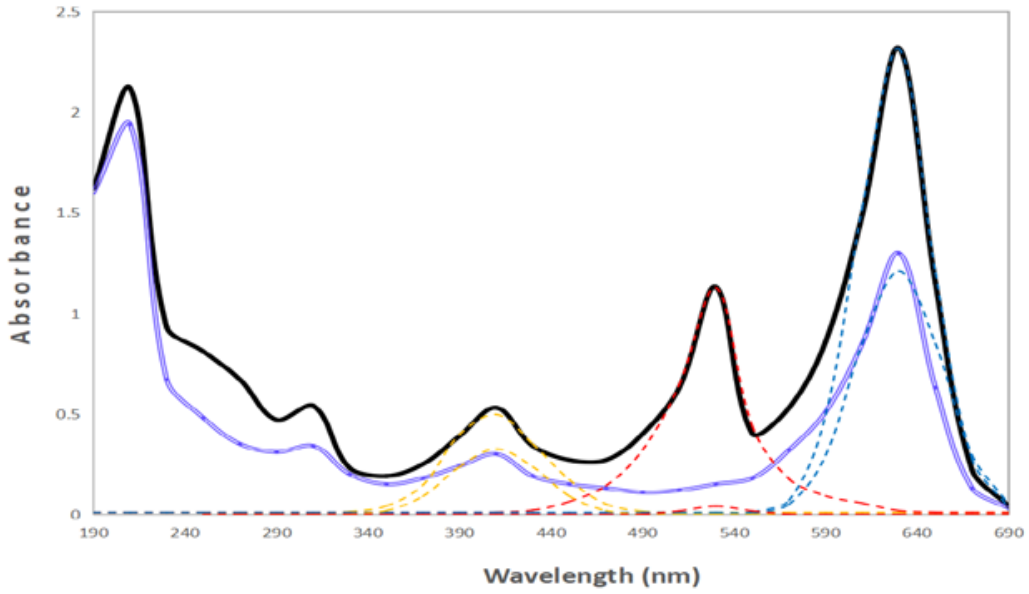

Figure 1. Comparison of UV-Vis spectra between the dye at 100% of the manufacturer's suggested concentration (black) and post-photoelectrochemical treatment (purple). Additionally, deconvoluted peaks associated with each dye are shown (dashed lines).

Additionally, an absorption region is observed in the near-ultraviolet wavelength region, indicating the dye's susceptibility to reacting in this range. The decreases in absorption at 428, 530, and 630 nm post-photoelectrochemical treatment are attributed to the reduction in dye concentration resulting from the breakage of chromophore bonds [28]. However, for a more in-depth analysis of the degradation process, the experimental design variables were examined through a multivariate analysis of variance (MANOVA).

The Table 2 presents the results of the multivariate analysis of variance (MANOVA) for the effect on the evaluated output parameters, considering imposed current, UV light, and their combined influence. The parameters studied included dye degradation, cell potential, recovered mass, and pH. Significant differences in the variance of these parameters at different imposed current values are evident, as indicated by the rejection of Roy's Largest Root statistical test with a probability level of zero.

Table 2. The MANOVA analysis results showcase the impact of imposed current, UV light, and their combination on the degradation of dyes, cell potential, recovered mass, and pH. The statistical examination reveals significant differences in the variance of these parameters under the influence of imposed current, UV light exposure, and their combined effect.

Statistical Test	Value of Test	GL1	GL2	Fraction F	Probability Level	Decision 0.15
Current (A)						
Roy's Largest Root	264.3	6	5	220.2	0.0	Reject
Tartrazine	786.6	3	8	30.3	0.00010	Reject
Erythrosine	446.2	3	8	25.0	0.00020	Reject
Brilliant Blue	1483.7	3	8	28.2	0.00013	Reject
Potential	140.8	3	8	366.9	0.0	Reject
Mass	0.014	3	8	34.3	0.000065	Reject
pH	0.063	3	8	6.0	0.019	Reject
UV Light (B)						
Roy's Largest Root	5.3	6	3	2.63	0.23	Accept
Tartrazine	69.3	1	8	2.67	0.14	Reject
Erythrosine	148.8	1	8	8.35	0.020	Reject
Brilliant Blue	46.6	1	8	0.89	0.37	Accept
Potential	1.8	1	8	4.75	0.061	Reject
Mass	0.0000040	1	8	0.01	0.92	Accept
pH	0.051756	1	8	4.87	0.058	Reject
Current-UV Light (AB)						
Roy's Largest Root	6.7	6	5	5.59	0.039	Reject
Tartrazine	78.5	3	8	3.02	0.094	Reject
Erythrosine	37.0	3	8	2.07	0.18	Accept
Brilliant Blue	174.7	3	8	3.32	0.078	Reject
Potential	0.35	3	8	0.92	0.47	Accept
Mass	0.00015	3	8	0.36	0.79	Accept
pH	0.091	3	8	8.58	0.007	Reject

On the other hand, the variance due to the imposition of UV light is accepted; however, it shows a statistical test with a low probability value (0.23), indicating a slight effect. This is evident in the changes in response parameters such as the degradation of Tartrazine and Erythrosine, as well as cell potential and pH, which exhibit significant variance when UV light is imposed. The combination of current and UV light primarily affects the degradation of Tartrazine and Brilliant Blue, and pH, with their variances being significantly different. It is noteworthy that no significant effects are observed in the variances in cell potential and recovered mass. This is because sediment production depends solely on the electrochemical process and is only dependent on the imposed current.

It should be noted that this study focused on evaluating the degradation process under controlled conditions, with temperature and UV intensity maintained as constant. The effect of temperature on reaction rates was considered based on Arrhenius behavior, while UV intensity was standardized using a commercially available system. Scaling up the technology and addressing the impact of these variables on a larger scale were not part of the scope of this work and would require further research.

4. Discussion

It can be highlighted that the adsorption mechanism of organic compounds onto metal oxides, such as alumina, likely follows similar pathways to those observed for the commercial dye degradation in the present study. Given that no significant shifts in peak values of maximum absorption, nor any evident bathochromic or hypochromic processes, were observed, the mechanism of capturing the organic compounds can be attributed to ligand exchange, surface complexation, and hydrophobic interactions, much like the sorption behavior of organic molecules onto metal oxide surfaces.

As seen in the case of alumina, organic molecules such as those present in the dye mixture may interact weakly through non-polar interactions, though more strongly when functional groups capable of complexation are involved. This interaction may result in the formation of surface complexes that influence the extent of degradation during photoelectrochemical treatment. Furthermore, the observed increase in sediment and precipitate mass could be attributed to the precipitation of degradation byproducts or the formation of insoluble complexes that are captured on the electrode or within the solution, thus affecting the overall dye degradation process. These changes in the sediment and precipitate mass support the notion that surface interactions are central to the observed effects on dye molecules under experimental conditions.

Figure 2 depicts the results of the evaluated parameters with and without UV light imposition (solid and dashed lines, respectively). The responses of the parameters are illustrated as follows: Figure 2a, fraction of dyes; Figure 2b, cell potential; Figure 2c, recovered mass; and Figure 2d, pH. In Figure 2a, the degraded fraction of each dye is shown, revealing that Erythrosine undergoes the highest degradation, followed by Tartrazine and Brilliant Blue. Additionally, an increase in the imposed current leads to greater degradation until reaching a plateau, indicating a mixed control of the reaction, initially electrochemical and subsequently photochemical. This is confirmed by observing higher degradation with UV light at higher imposed current values, suggesting photoelectrochemical control beyond 1 mA cm^{-2}.

Figure 2b displays the potentiometric analysis results during current imposition, with and without UV light (solid and dashed lines, respectively). In both cases, the potential increases with current, reaching a stabilization plateau from 1 mA $\times$ cm^{-2} onwards, transitioning from charge transfer-limited to the availability of anode sites for oxidation. Notably, the cell potential is lower when UV light is imposed, suggesting that UV light contributes to the reaction's energy requirements. The observed behavior indicates that the system shifts from being limited by the electrochemical processes at lower currents to being governed by the availability of active sites on the anode at higher currents. The presence of UV light seems to reduce the overall energy demand of the system, potentially enhancing the oxidation of the dye molecules through synergistic photochemical reactions.

The effect of current density on various parameters such as the fraction of degraded dyes, cell potential, recovered mass, and pH should be explored in greater detail. The current density plays a crucial role in determining the rate of degradation and the efficiency of the process. A higher current density typically leads to an increase in the production of reactive species, which enhances the degradation rate of the dyes but may also alter the pH, affecting the overall process efficiency. The relationship between current density and the fraction of degraded dyes is often nonlinear, with an optimal current density beyond which the efficiency may plateau or decrease due to side reactions or excessive energy consumption. Additionally, the recovered mass and pH should be analyzed to provide insight into the material balance and the chemical dynamics occurring during the degradation process.

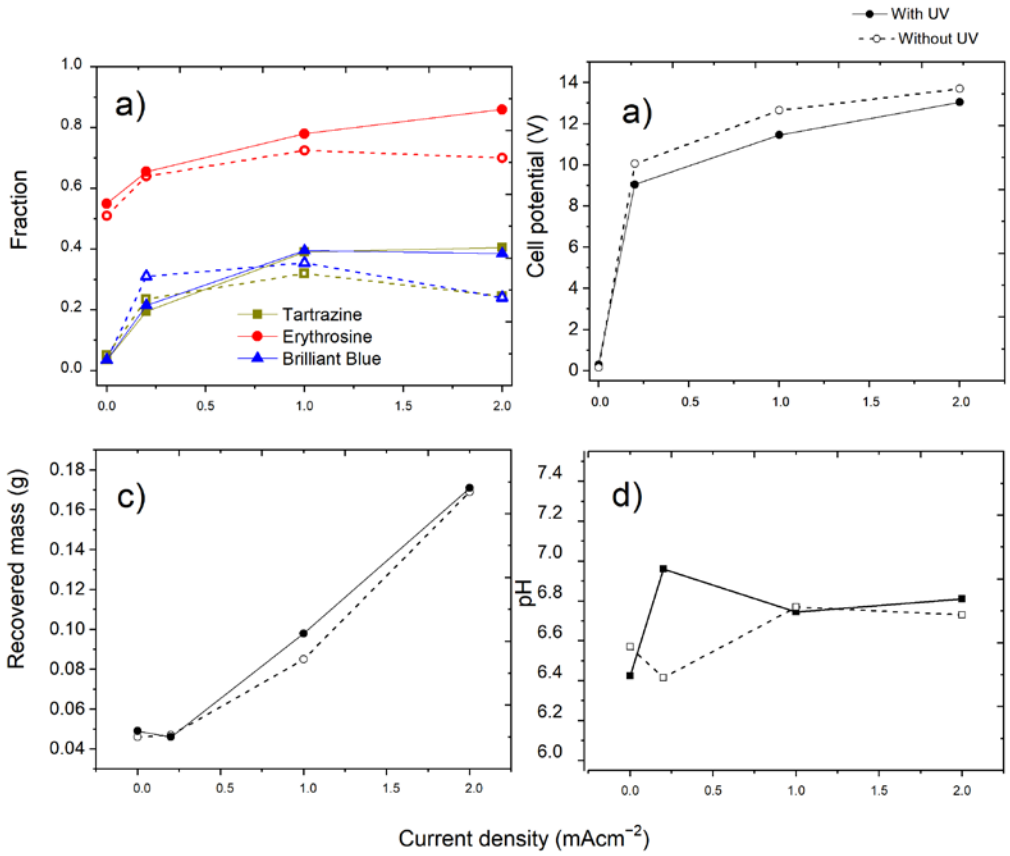

Figure 2. Effect with (solid line) and without imposition (dashed line) of UV light and imposed current on (**a**) dye degradation, (**b**) cell potential, (**c**) recovered mass, and (**d**) pH.

Figure 2c presents results from gravimetric analysis during current imposition, with and without UV light (solid and dashed lines, respectively). The solids formed and dispersed inside the reactor are associated with oxides formed at the anode. These solids are responsible for flocculating organic dye molecules, and the amount of solid produced is proportional to the TiO_2 generated electrochemically. The slope is observed to be 0.63 g $\times$ mA^{-1} $\times$ cm^2, indicating a consistent relationship regardless of UV light imposition. Additionally, a slight increase in mass associated with heterogeneous flocculation of dyes is observed with UV light.

Figure 2d illustrates the results of pH potentiometric analysis during current imposition, with and without UV light (solid and dashed lines, respectively). In both cases, a slight increase in pH with imposed current is observed due to the modification of the chemical composition of the solution.

On the other hand, Figure 3 illustrates the degradation kinetics with and without the imposition of ultraviolet light (blue squares and red circles, respectively). Experimental data without UV light imposition were fitted using Equation (3), while Equation (4) was employed for fitting the data with UV light.

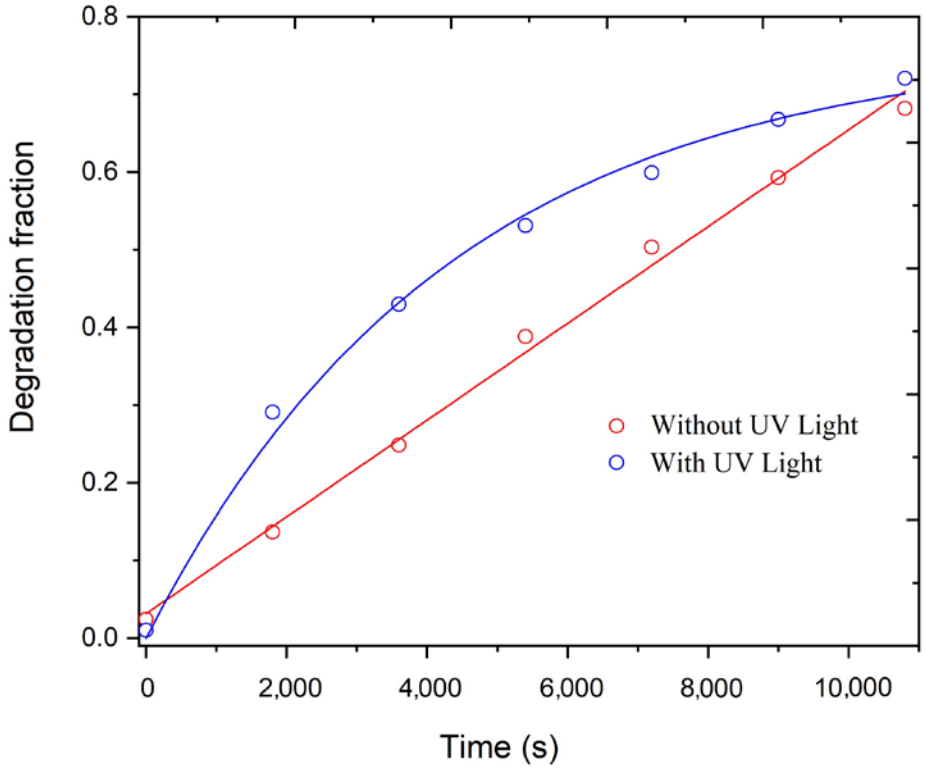

Figure 3. Reaction kinetics of the process with UV light imposition (blue squares) and without UV light (red circles), along with their fits using the kinetic models; electrochemical and photoelectrochemical (solid lines).

The kinetics observed in the electrochemical process without UV light is of zero order and relies on the electrolytic reaction of Ti^{2+} production (Equation (5)) along with the chemical oxidation reaction of Ti^{2+} with water to form TiO_2 (Equation (6)). Therefore, its electrochemical rate law (Equation (7)) can be expressed as the sum of both oxidation rates 1 and 2, yielding an electrochemical constant K_{el}. This is expressed as the sum of the inverses of oxidation constants 1 and 2. Finally, by solving the differential equation of Equation (5), Equation (8) can be obtained, representing the kinetics.

$$Ti_s \rightarrow Ti^{2+} + 2e^- \tag{5}$$

$$Ti^{2+} + 2H_2O \rightarrow TiO_2 + 2e^- + 4H^+ \tag{6}$$

$$v_{el} = \frac{d[TiO_2]}{dt} = (k_{ox_1} + k_{ox_2})\frac{j}{zFA} \tag{7}$$

$$[n]_t = [n]_0 - K_{el}\frac{jA}{zF}\,t \tag{8}$$

On the other hand, for fitting the data when UV light is imposed, the activation of TiO_2 (hν) (Reaction 9) and its subsequent reaction with the dye (Reaction 10) are considered. Therefore, Reaction 11 represents the overall reaction of the reactor's operation, and its rate law is expressed in Equation (12).

$$TiO_2 + h\nu \rightarrow TiO_2(h\nu) \tag{9}$$

$$TiO_2(h\nu) + n \rightarrow \ TiO_2 + Degradation \tag{10}$$

$$Ti_s + 2H_2O + h\nu + Dye \rightarrow \ \ TiO_2 + Degradation + 4e^- + 4H^+ \tag{11}$$

$$v_{fel} = \left(\frac{1}{k_{ox_1}} + \frac{1}{k_{ox_2}}\right)\frac{jA}{zF} + k_{hv}[TiO_2(hv)] + k_{deg}[TiO_2][Degradation] \quad (12)$$

To solve Equation (12), the theory of activated complex is considered, where the concentrations of TiO_2 (hν) and Ti^{2+} are constants, and their formation and consumption rates are assumed to be zero. For this, the chemical equilibrium of Reaction 6 is considered, as shown in Equation (13), and the value of the TiO_2 concentration in terms of Ti^{2+} is obtained in Equation (14). Meanwhile, the concentration of Ti^{2+} is obtained by considering its rate to be zero and is expressed in Equation (15), as its production and consumption are equal, representing the concentration of Ti^{2+} in Equation (16).

$$k_{ox_2}\left[Ti^{2+}\right] = k_{red_2}[TiO_2] \quad (13)$$

$$[TiO_2] = \frac{k_{ox_2}\left[Ti^{2+}\right]}{k_{red_2}} \quad (14)$$

$$v_{Ti^{2+}} = \frac{1}{k_{ox_1}}\frac{jA}{zF} - k_{ox_1}\left[Ti^{2+}\right] \quad (15)$$

$$\left[Ti^{2+}\right] = \frac{1}{k_{ox_2}k_{ox_1}}\frac{jA}{zF} \quad (16)$$

By substituting Equations (14) and (16) into Equation (12), it is possible to obtain the velocity equation for the photoelectrochemical reaction, as shown in Equation (17). This can be further simplified (Equation (18)) by considering two generalized constants: the electrochemical constant $K_{el}{}'$ and the photoelectrochemical constant K_{fel}.

$$v_{fel} = \left(\frac{1}{k_{ox_1}} + \frac{1}{k_{ox_2}}\right)\frac{jA}{zF} - 2\frac{k_{deg}}{k_{ox_1}k_{red_2}}\frac{jA}{zF}[Deg] \quad (17)$$

$$v_{fel} = K_{el}{}'\frac{jA}{zF} - 2K_{fel}\frac{jA}{zF}[Deg] \quad (18)$$

Finally, using the integration method, Equation (19) is obtained, which represents the concentration of the degraded dye as a function of time (Equation (19)). Equations (20) and (21) describe key parameters in the kinetic modeling of dye degradation in the photoelectrochemical reactor. Equation (20) relates the global efficiency constant (k_{el}) to the product of the first-order and second-order oxidation constants (k_{ox1} and k_{ox2}) and the adjusted efficiency constant ($K_{el}{}'$). This highlights the role of oxidation processes in determining efficiency.

Equation (21) defines the global degradation constant (k_{deg}) as the product of the first-order oxidation constant (k_{ox1}) and the second-order reduction constant (k_{red2}), scaled by the fast electron transfer constant (k_{fel}). It emphasizes the interplay between oxidation and reduction reactions in the degradation process. These equations provide insights into the reaction mechanisms and contribute to optimizing operational parameters.

$$[Deg] = \frac{K_{el}{}'}{K_{fel}} - e^{K_{fel}\frac{jA}{zF}t} \quad (19)$$

$$K_{el} = (k_{ox_1}k_{ox_2})K_{el}{}' \quad (20)$$

$$k_{deg} = \left(k_{ox_1}k_{red_2}\right)K_{fel} \quad (21)$$

The experimental data were fitted using Equations (8) and (19) for processes without and with ultraviolet light imposition, respectively. In Figure 3, the fraction of degraded dye over time is shown, obtaining values for the electrochemical process (without UV light)

of the K_{el}' constant as 22.39 ± 0.49 mL × L^{-1} of dye, with an adjustment of experimental data to the mathematical model of 0.9893. Meanwhile, for the process with UV light, K_{el}' presents values of 27.2 ± 3.3 mL × L^{-1}, and K_{fel} presents values of 25.78 ± 3.7 mL × L^{-1}, with an adjustment of experimental data to the mathematical model of 0.9360. As observed, the value of K_{el}' is like that obtained with the electrochemical process, and the value of K_{fel} is of a similar magnitude.

Further analysis reveals significant differences in the oxidation and reduction constants for both processes. For the process without UV light, the first-order oxidation constant k_{ox1} was 0.035 ± 0.004 mL × L^{-1}, while the second-order oxidation constant k_{ox2} reached 22.36 ± 0.49 mL × L^{-1}. Similarly, the reduction constant K_{red2} was determined to be 23.5 ± 6.2 s^{-1}. The overall degradation rate constant k_{deg} was 21.2 ± 4.0 s^{-1}, highlighting the efficiency of the process under these conditions. The incorporation of UV light enhanced the degradation process, as evidenced by the increased values of k_{el} and k_{fel}, suggesting that UV light facilitates additional photochemical pathways or promotes faster electron transfer at the surface. These results underscore the importance of ultraviolet light in improving the efficiency of photoelectrochemical reactors for dye degradation.

Overall, the combination of kinetic and efficiency parameters confirms the effectiveness of the proposed reactor design and provides a robust foundation for optimizing operational conditions. Future studies could explore additional variations in operational parameters, such as current density and light intensity, to further improve the reactor's performance. The photoelectrochemical reactor offers the advantage of rapid degradation kinetics at the start of the process. However, as the reaction progresses, the rate slows and may eventually align with conventional processes. This difference in kinetics—initially fast, then logarithmic—could pose challenges in batch reactors due to diminishing degradation efficiency over time. However, this could be an advantage in continuous flow reactors, where the high initial degradation rate would ensure efficient treatment without requiring long residence times, making it a promising option for large-scale industrial applications.

Finally, the efficiency parameters of the batch reactor were evaluated for its operation without and with UV light, respectively. As observed in Table 3, the cell potentials are 13.7 and 13.05 V, respectively, and the decrease can be attributed to the contribution of ultraviolet energy in the electrochemical system operation. The energy consumption per unit of degraded mass has values of 6.20 and 3.71 kW × h × kg^{-1}, and it can be noted that the photoelectrochemical system demonstrates better efficiency within the same effective area of 33.3 m^{-1}. Meanwhile, the space–time efficiency presents 31.6 and 52.73 g × mL × h^{-1}, achieving a degradation of 1.7 times more dyes using the same amount of electrical current density.

Advanced oxidation processes (AOPs) such as UV/H_2O_2 have proven highly effective in degrading textile dyes. Radović et al. (2015) demonstrated that the photo-Fenton process outperformed the UV/H_2O_2 and Fenton methods in decolorizing Reactive Orange 4 and Reactive Blue 19. Similarly, Mitrović et al. (2019) emphasized the role of sulfate radicals, generated via UV-C-activated peroxydisulfate, in improving dye degradation. Petrović et al. (2022) showcased the effectiveness of plasma-modified CeO_2 catalysts for catalytic and photocatalytic dye removal, achieving significant Total Organic Carbon (TOC) reduction and process stability.

Table 3. Efficiency parameters of the batch photoelectrochemical reactor during operation without and with ultraviolet light. Values are shown for cell potential, electrical consumption per unit of degraded mass, effective area, space–time efficiency, and current density.

Kinetics and Efficiency Parameters	Without UV Light	With UV Light
$k_{el}/mL \times L^{-1}$	22.39 ± 0.49	--
$k_{el}'/mL \times L^{-1}$	n/a	27.2 ± 3.3
k_{fel}/s^{-1}	n/a	25.78 ± 3.7
$K_{ox1}/mL \times L^{-1}$	0.035 ± 0.004	
$K_{ox2}/mL \times L^{-1}$	22.36 ± 0.49	
K_{red2}/s^{-1}	23.5 ± 6.2	
K_{deg}/s^{-1}	21.2 ± 4.0	
E_{cell}/V	13.70	13.05
E_{cell}/V	13.70	13.05
Consumption/$kW \times h \times kg^{-1}$	6.20	3.71
$\tau_{et}/g \times mL \times h^{-1}$	31.6	52.73
$j/A \times m^{-2}$	20	

In comparison, the current study explores an electrochemical approach, both with and without UV light, achieving competitive degradation rates and efficiency parameters. Unlike traditional AOPs like UV/H_2O_2 and photocatalytic methods, this electrochemical system utilizes anodic and cathodic reactions to degrade dyes. While AOPs such as photo-Fenton and plasma-catalysis have demonstrated strong performance, they often depend on specific reagents, catalysts, or irradiation conditions that may hinder their scalability. In contrast, the electrochemical method studied here offers operational simplicity and adaptability, making it a promising complementary technology for wastewater treatment. Furthermore, this approach can be optimized for continuous flow systems, where the synergy between electrochemical and UV activation presents a significant operational advantage.

This electrochemical method provides a more flexible and scalable option compared to conventional AOPs. By leveraging anodic and cathodic reactions in combination with UV light, the system offers advantages in terms of operational simplicity, adaptability, and potential for integration into continuous flow reactors. This characteristic makes it an attractive alternative for large-scale wastewater treatment applications, where efficiency and cost-effectiveness are critical. Additionally, its ability to operate without the need for specific reagents or catalysts enhances its applicability across a wide range of wastewater types.

5. Conclusions

The conclusions are valid, but they could be expanded to include more practical implications and avenues for future research. This study demonstrates that photoelectrochemical treatment, with a current density of 20 $A \times cm^{-2}$ and UV light, significantly affects the degradation of the studied dye. The reduction in absorption of the dye's characteristic bands after treatment indicates the breaking of chromophore bonds and a decrease in dye concentration. Multivariate analysis revealed significant differences in dye degradation, cell potential, recovered mass, and pH based on varying current densities. The combination of UV light and current induced further changes in dye degradation, cell potential, and pH, highlighting the synergistic effect of UV light in the degradation process.

While these findings suggest that photoelectrochemical treatment with current and UV light can be a promising strategy for dye degradation in aqueous solutions, the study's limitations must be acknowledged. Specifically, factors such as the effect of temperature and UV intensity, which are known to influence degradation, were controlled but not further explored in terms of scaling up for industrial applications. The study's scope did not address large-scale implementation, which would require additional research to understand technical challenges and optimize conditions for practical use. Future research should focus on refining these treatment parameters, investigating the degradation mechanisms in more detail, and exploring potential industrial applications of photoelectrochemical technologies for wastewater treatment and the removal of colored contaminants.

Author Contributions: Conceptualization, D.I.C.-L., A.O.-M., V.E.R.-C., M.R.-P., F.M.G.-M. and J.A.C.-M.; Methodology, D.I.C.-L., A.O.-M., V.E.R.-C., M.R.-P., M.V., N.T., J.A.C.-M. and F.M.G.-M.; software, D.I.C.-L., A.O.-M., V.E.R.-C., M.R.-P. and J.A.C.-M.; validation, D.I.C.-L., A.O.-M., V.E.R.-C., M.R.-P., J.A.C.-M. and F.M.G.-M.; formal analysis, D.I.C.-L., A.O.-M., V.E.R.-C., M.R.-P., J.A.C.-M., S.L.-G. and F.M.G.-M.; resources, J.A.C.-M. and F.M.G.-M.; data curation, D.I.C.-L., A.O.-M., V.E.R.-C., M.R.-P. and J.A.C.-M.; writing-original draft preparation, D.I.C.-L., A.O.-M., V.E.R.-C., M.R.-P., J.A.C.-M., S.L.-G., M.V., N.T. and F.M.G.-M.; writing review and editing, D.I.C.-L., A.O.-M., V.E.R.-C., M.R.-P., J.A.C.-M., S.L.-G., M.V., N.T. and F.M.G.-M.; visualization, D.I.C.-L., A.O.-M., V.E.R.-C., M.R.-P., J.A.C.-M., S.L.-G., M.V., N.T. and F.M.G.-M.; supervision, J.A.C.-M. and F.M.G.-M.; project administration, J.A.C.-M. and F.M.G.-M.; funding acquisition, F.M.G.-M. and M.V. All authors have read and agreed to the published version of the manuscript.

Funding: This research received no external funding.

Institutional Review Board Statement: Not applicable.

Informed Consent Statement: Not applicable.

Data Availability Statement: The original contributions presented in the study are included in the article, further inquiries can be directed to the corresponding authors.

Acknowledgments: The authors would like to thank the Programa de Doctorado en Energía Solar of the Universidad de Antofagasta, Chile; and the support of ANID-Chile through the research project FONDECYT Iniciación 11230550; and ANID/FONDAP 1522A0006 Solar Energy Research Center SERC-Chile.

Conflicts of Interest: The authors declare no conflicts of interest.

References

1. Beluci, N.D.C.L.; Homem, N.C.; Amorim, M.T.S.P.; Bergamasco, R.; Vieira, A.M.S. Biopolymer extracted from Moringa oleifera Lam. in conjunction with graphene oxide to modify membrane surfaces. *Environ. Technol.* **2020**, *41*, 3069–3080. [CrossRef]
2. Ferreira, A.; Ribeiro, B.; Ferreira, A.F.; Tavares, M.L.; Vladic, J.; Vidović, S.; Cvetkovic, D.; Melkonyan, L.; Avetisova, G.; Goginyan, V.; et al. Scenedesmus obliquus microalga-based biorefinery—From brewery effluent to bioactive compounds, biofuels and biofertilizers—Aiming at a circular bioeconomy. *Biofuels Bioprod. Biorefining* **2019**, *13*, 1169–1186. [CrossRef]
3. Januário, E.F.D.; Vidovix, T.B.; Beluci, N.D.C.L.; Paixão, R.M.; da Silva, L.H.B.R.; Homem, N.C.; Bergamasco, R.; Vieira, A.M.S. Advanced graphene oxide-based membranes as a potential alternative for dyes removal: A review. *Sci. Total Environ.* **2021**, *789*, 147957. [CrossRef] [PubMed]
4. Saha, P.; Bhaskara, R. Immobilization as a powerful bioremediation tool for abatement of dye pollution: A review. *Environ. Rev.* **2021**, *29*, 277–299. [CrossRef]
5. Mahmoud, G.A.; Ismail, L.M. Photocatalytic degradation of Direct Yellow 50 on TiO2 and Fe3+-doped TiO2 semiconductor nanoparticles under UV light irradiation. *J. Am. Sci.* **2012**, *8*, 83–99.
6. Hachem, C.; Bocquillon, F.; Zahraa, O.; Bouchy, M. Decolourization of textile industry wastewater by the photocatalytic degradation process. *Dye. Pigment.* **2001**, *49*, 117–125. [CrossRef]
7. Kalia, S.; Dalvi, V.; Kumar Nair, V.; Samuchial, S.; Malik, A. Hybrid electrocoagulation and laccase mediated treatment for efficient decolorization of effluent generated from textile industries. *Environ. Res.* **2023**, *228*, 115868. [CrossRef]

8. Bizani, E.; Fytianos, K.; Poulios, I.; Tsiridis, V. Photocatalytic decolorization and degradation of dye solutions and wastewaters in the presence of titanium dioxide. *J. Hazard. Mater.* **2006**, *136*, 85–94. [CrossRef]
9. Tu, Y.; Xiong, Y.; Descorme, C.; Kong, L.; Tian, S. Heterogeneous photo-Fenton oxidation of Acid Orange II over iron–sewage sludge derived carbon under visible irradiation. *J. Chem. Technol. Biotechnol.* **2013**, *89*, 544–551. [CrossRef]
10. Körbahti, B.K.; Rauf, M.A. Application of response surface analysis to the photolytic degradation of Basic Red 2 dye. *Chem. Eng. J.* **2008**, *138*, 166–171. [CrossRef]
11. Shu, H.Y.; Huang, C.R.; Chang, M.C. Decolorization of mono-azo dyes in wastewater by advanced oxidation process: A case study of acid red 1 and acid yellow 23. *Chemosphere* **1994**, *29*, 2597–2607. [CrossRef]
12. Marugán, J.; López Muñoz, M.J.; Grieken, R.V.; Aguado, J. Photocatalytic Decolorization and Mineralization of Dyes with Nanocrystalline TiO2/SiO2 Materials. *Ind. Eng. Chem. Res.* **2007**, *46*, 7605–7610. [CrossRef]
13. Gupta, V.K.; Jain, R.; Nayak, A.; Agarwal, S.; Shrivastava, M. Removal of the hazardous dye—Tartrazine by photodegradation on titanium dioxide surface. *Mater. Sci. Eng. C* **2011**, *31*, 1062–1067. [CrossRef]
14. Márquez-Ramírez, E.; Michtchenko, A.; Zacahua-Tlacuatl, G. Effects of radiation of co_2 laser on natural dolomite for the degradation of azo dye reactive black 5 by photocatalysis. *Rev. Mex. Ing. Química* **2019**, *18*, 555–569. [CrossRef]
15. Radović, M.D.; Mitrović, J.Z.; Kostić, M.M.; Bojić, D.V.; Petrović, M.M.; Najdanović, S.M.; Bojić, A.L. Comparison of ultraviolet radiation/hydrogen peroxide, Fenton and photo-Fenton processes for the decolorization of reactive dyes. *Hem. Ind.* **2015**, *69*, 657–665. [CrossRef]
16. Nidheesh, P.V.; Gandhimathi, R. Comparative Removal of Rhodamine B from Aqueous Solution by Electro-Fenton and Electro-Fenton-Like Processes. *Clean* **2014**, *42*, 779–784. [CrossRef]
17. Mitrović, J.; Vučić, M.R.; Kostić, M.; Velinov, N.; Najdanović, S.; Bojić, D.; Bojić, A. Sulfate radicals-based degradation of antraquinone textile dye in a plug flow photoreactor. *J. Serbian Chem. Soc.* **2019**, *89*, 1041–1054. [CrossRef]
18. Petrović, M.; Jovanović, T.; Rančev, S.; Kovač, J.; Velinov, N.; Najdanović, S.; Kostić, M.; Bojić, A. Plasma modified electrosynthesized cerium oxide catalyst for plasma and photocatalytic degradation of RB 19 dye. *J. Environ. Chem. Eng.* **2022**, *3*, 107931. [CrossRef]
19. Kokkinos, P.; Venieri, D.; Mantzavinos, D. Advanced Oxidation Processes for Water and Wastewater Viral Disinfection. A Systematic Review. *Food Environ. Virol.* **2021**, *13*, 283–302. [CrossRef] [PubMed]
20. Thiam, A.; Zhou, M.; Brillas, E.; Sirés, I. Two-step mineralization of Tartrazine solutions: Study of parameters and by-products during the coupling of electrocoagulation with electrochemical advanced oxidation processes. *Appl. Catal. B Environ.* **2014**, *150*, 116–125. [CrossRef]
21. Emmanuel, S.S.; Adesibikan, A.A.; Saliu ODOpatola, E.A. Greenly biosynthesized bimetallic nanoparticles for ecofriendly degradation of notorious dye pollutants: A review. *Plant Nano Biol.* **2023**, *3*, 100024. [CrossRef]
22. Jhones dos Santos, A.; Sirés, I.; Martínez-Huitle, C.A.; Brillas, E. Total mineralization of mixtures of Tartrazine, Ponceau SS and Direct Blue 71 azo dyes by solar photoelectro-Fenton in pre-pilot plant. *Chemosphere* **2018**, *18*, 1137–1144. [CrossRef] [PubMed]
23. Suliman, Z.A.; Mecha, A.C.; Mwasiagi, J.I. Effect of TiO2/Fe2O3 nanopowder synthesis method on visible light photocatalytic degradation of reactive blue dye. *Heliyon* **2024**, *10*, E29648. [CrossRef] [PubMed]
24. Miklos, D.; Remy, C.; Jekel, M.; Linden, K.G.; Drewes, J.E. Evaluation of advanced oxidation processes for water and wastewater treatment—A critical review. *Water Res.* **2018**, *139*, 118–131. [CrossRef] [PubMed]
25. Sharifzade, C.; Asghari, A.; Rajabi, M. Highly effective adsorption of xanthene dyes (rhodamine B and erythrosine B) from aqueous solutions onto lemon citrus peel active carbon: Characterization, resolving analysis, optimization and mechanistic studies. *RSC Adv.* **2017**, *7*, 5362. [CrossRef]
26. Ramakrishnan, S.P.; Bagya Lakshmi, J.; Surya, P.R. Estimation of synthetic dye erythrosine in food stuff and formulation and effect of dye on the protein binding of drug in BSA. *Pharm. Lett.* **2011**, *3*, 361–373.
27. Liu, Y.; Hua, L.; Li, S. Photocatalytic degradation of Reactive Brilliant Blue KN-R by TiO2/UV process. *Desalination* **2010**, *258*, 48–53. [CrossRef]
28. He, D.; Chen, Y.; Situ, Y.; Zhong, L.; Huang, H. Synthesis of ternary g-C3N4/Ag/γ-FeOOH photocatalyst: An integrated heterogeneous Fenton-like system for effectively degradation of azo dye methyl orange under visible light. *Appl. Surf. Sci.* **2017**, *425*, 862–872. [CrossRef]

Disclaimer/Publisher's Note: The statements, opinions and data contained in all publications are solely those of the individual author(s) and contributor(s) and not of MDPI and/or the editor(s). MDPI and/or the editor(s) disclaim responsibility for any injury to people or property resulting from any ideas, methods, instructions or products referred to in the content.